HHS Public Access

Author manuscript

Neuroimage. Author manuscript; available in PMC 2016 November 01.

Published in final edited form as:

Neuroimage. 2015 November 1; 121: 253–262. doi:10.1016/j.neuroimage.2015.07.049.

Preclinical evaluation of a promising C-11 labeled PET tracer for imaging phosphodiesterase10A in the brain of living subject

Hui Liu[1], **Hongjun Jin**[1], **Xuyi Yue**[1], **Xiang Zhang**[1], **Hao Yang**[1], **Junfeng Li**[1], **Hubert Flores**[2], **Yi Su**[2], **Joel S. Perlmutter**[1,2,3], and **Zhude Tu**[1,*]

[1]Department of Radiology, Washington University School of Medicine, St. Louis, MO 63110, USA

[2]Department of Neurology, Washington University School of Medicine, St. Louis, MO 63110, USA.

[3]Department of Neurobiology, Physical Therapy and Occupational Therapy, Washington University School of Medicine, St. Louis, MO 63110, USA

Abstract

Phosphodiesterase 10A (PDE10A) plays a key role in the regulation of brain striatal signaling. A PET tracer for PDE10A may serve as a tool to evaluate PDE10A expression *in vivo* in central nervous system disorders with striatal pathology. Here, we further characterized the binding properties of a previously reported radioligand we developed for PDE10A, [^{11}C]**TZ1964B**, in rodents and nonhuman primates (NHPs). The tritiated counterpart [^{3}H]**TZ1964B** was used for *in vitro* binding characterizations in rat striatum homogenates and *in vitro* autoradiographic studies in rat brain slices. The carbon-11 labeled [^{11}C]**TZ1964B** was utilized in the *ex vivo* autoradiography studies for the brain of rats and microPET imaging studies for the brain of NHPs. MicroPET scans of [^{11}C]**TZ1964B** in NHPs were conducted at baseline, as well as with using a selective PDE10A inhibitor MP-10 for either pretreatment or displacement. The *in vivo* regional target occupancy (Occ) was obtained by pretreating with different doses of MP-10 (0.05 - 2.00 mg/kg). Both *in vitro* binding assays and *in vitro* autoradiographic studies revealed a nanomolar binding affinity of [^{3}H]**TZ1964B** to the rat striatum. The striatal binding of [^{3}H]**TZ1964B** and [^{11}C]**TZ1964B** was either displaced or blocked by MP-10 in rats and NHPs. Autoradiography and microPET imaging confirmed that the specific binding of the radioligand was found in the striatum but not in the cerebellum. Blocking studies also confirmed the suitability of the cerebellum as an appropriate reference region. The binding potentials (BP_{ND}) of [^{11}C]**TZ1964B** in the NHP striatum that were calculated using either the Logan reference model (LoganREF, 3.96 ± 0.17) or the simplified reference tissue model (SRTM, 4.64 ± 0.47), with the cerebellum as the reference region, was high and had good reproducibility. The occupancy studies indicated a MP-10 dose of 0.31 ± 0.09 mg/kg (LoganREF) / 0.45 ± 0.17 mg/kg (SRTM) occupies 50% striatal PDE10A binding sites.

*Corresponding author. Tel.: +1-314-362-8487; Fax: +1-314-362-8555; tuz@mir.wustl.edu.

Disclosure

The authors do not have any conflict of interest.

Studies in rats and NHPs demonstrated radiolabelled **TZ1964B** has a high binding affinity and good specificity for PDE10A, as well as favorable *in vivo* pharmacokinetic properties and binding profiles. Our data suggests that [^{11}C]**TZ1964B** is a promising radioligand for *in vivo* imaging PDE10A in the brain of living subject.

Keywords

PDE10A; radioligand; microPET; C-11; H-3; brain imaging; binding assay; autoradiography

1. Introduction

Phosphodiesterase 10A (PDE10A) is expressed primarily in the medium spiny neurons (MSNs) of the striatum, which is a major input site into basal ganglia of the mammalian brain (Soderling et al., 1999; Strick, 2010). Nigrostriatal terminals release dopamine that engages dopaminergic receptors on MSNs. These receptor interactions lead to changes in cyclic nucleotides mediated by PDE10A. Dysfunction of nigrostriatal transmission and MSN function contributes to multiple neurologic and psychiatric illnesses and may provide novel targets for therapeutic interventions (Nishi et al., 2011). Thus, PDE10A may serve as a reliable biomarker for disease progression or a potential target for therapeutic interventions in various central nervous system (CNS) diseases, such as Parkinson disease, schizophrenia, Huntington disease, and addiction (Celen et al., 2013). Moreover, molecular imaging of PDE10A by PET provides a potential *in vivo* biomarker of striatal PDE10A function.

Over the past 10 years, tremendous efforts have been made to develop specific PET tracers for imaging PDE10A in the brain. Our group firstly reported the synthesis of a PDE10A PET radiotracer, carbon-11 radiolabeled papaverine (PDE10A inhibition IC_{50} = 36 nM) in 2010 (Tu et al., 2010). Due to the low retention of the tracer ([^{11}C]papaverine) in rat and monkey striatum, the more potent and specific PDE10A inhibitor MP-10 (IC_{50} = 0.18 nM) was selected for radiolabelling. However, a radiolabeled metabolite capable of penetrating the blood–brain-barrier limits the clinical utility of [^{11}C]MP-10 for PET quantification of PDE10A (Plisson et al., 2011; Tu et al., 2011). Recently our group reported a series of pyrazole group-containing analogues with a methoxy group on the quinoline fragment, which displayed high potency and selectivity for PDE10A (Li et al., 2013). Among these compounds, **TZ1964B** has high PDE10A binding potency with an IC_{50} value of 0.40 ± 0.02 nM and high selectivity for PDE10A versus PDE3A/3B and PDE4A/4B with IC_{50} > 1500 nM (Li et al., 2013). Biodistribution in normal rats and MP-10 pretreatment in rats revealed that [^{11}C]**TZ1964B,** named as [^{11}C]1 previously, had high striatal accumulation and good binding specificity for PDE10A (Fan et al., 2014). MicroPET studies in nonhuman primates (NHP) consistently showed good tracer retention in the striatum with rapid clearance from non-target brain regions, and a stable metabolism profile that only one hydrophilic radiometabolite was detected (Fan et al., 2014).

In the present study, we further evaluated the *in vitro* binding properties of the ligand using its tritiated counterpart [^{3}H]**TZ1964B**, and characterized the *in vivo* tracer kinetics and

binding characteristics of [^{11}C]**TZ1964B** in the brains of NHPs, to determine whether this radioligand could permit quantification of PDE10A availability.

2. Materials and methods

2.1 Radioligand preparation

The tritiated compound was custom synthesized by American Radiolabeled Chemicals, Inc. (St. Louis, MO). The carbon-11 labeled compound [^{11}C]**TZ1964B** was successfully synthesized through *O*-methylation of the corresponding precursor, following our previous report (Fan et al., 2014).

2.2 Compound preparation

Reagents and standard compounds for *in vitro* binding assays were purchased from Sigma (St. Louis, MO) and Tocris Biosciences (R&D Systems, Minneapolis, MN). Novel compounds were synthesized in-house. Test compounds (**Table 1**) were dissolved in *N*,*N*-dimethylformamide (DMF) or ethanol to create a stock solution; the desired concentration for *in vitro* assays was subsequently obtained by further dilution in the Tris-HCl assay buffer (50 mM Tris/HCl, 8.30 mM $MgCl_2$, 1 mM EDTA, pH 7.5). In the blocking and displacement studies of microPET scans, the solution of MP-10 (0.50 mg/mL) was achieved with 10% PEG300/30% cyclodextrin solution/60% water.

2.3 Experimental animals

All animal experiments were conducted in compliance with the Guidelines for the Care and Use of Research Animals under protocols approved by Washington University's Animal Studies Committee. Mature, male Sprague–Dawley (SD) rats (Charles River Laboratories, Inc., Wilmington, MA) were used for *in vitro* binding assays and *in vitro* autoradiography. Tail vein injections were performed under light inhalation anesthesia (1-2% isoflurane/oxygen) and euthanasia was done under surgical plane anesthesia. Two male adult cynomolgus monkeys, weighing on average 4-6 kg, served as subjects for microPET studies.

2.4 *In vitro* binding assay in rat brain homogenates

2.4.1 Brain homogenate preparation—Subcellular fraction was carried out as described by Xie et al. (Xie et al., 2006). Rats were euthanized, and bilateral striatum were dissected and homogenized. Tissue homogenization was carried out in cold (4 °C) homogenization buffer (0.32 M sucrose, 4 mM HEPES-NaOH, 1 mM EDTA, pH 7.4) by vigorous vortexing. The homogenate was then centrifuged for 10 min at 800×g to yield the pellet (P0) and the supernatant (S0). P0 was washed in five volumes of lysis buffer, centrifuged again to yield P1 and S1. S0 and S1 were pooled and centrifuged for 15 min at 9000×g yielding S2 and P2. The supernatant S2 was further spun at 100,000 × g for 60 min using the Beckman Ti45 rotor to yield the high speed membrane fraction P20. P20 was re-suspended into the Tris-HCl assay buffer. Aliquots were stored at −80 °C until use. The protein concentration of the suspension was determined using the DC protein assay (Bio-Rad, Hercules, CA).

2.4.2 Radioligand binding assay—The kinetic analysis of [^{3}H]**TZ1964B** (~2 nM) binding to rat striatum homogenates P20 (~80 μg /ml) was carried out to measure the association (K_{on}) and dissociation (K_{off}) rates. Association and dissociation curves were obtained by recording the amount of the radioligand bound specifically as a function of time at a constant concentration of both the radioligand and the enzyme. Dissociation experiments were carried out by adding 10 μM of MP-10 to the reaction mixture after equilibrium was achieved and the specific binding of the radioligand as a function of time was determined. The values of K_{on} and K_{off} were determined by nonlinear regression analysis using GraphPad Prism 5.0 (GraphPad Software, Inc., San Diego, CA).

For the saturation binding assay, rat striatum homogenates P20 were diluted and incubated for 60 min with [^{3}H]**TZ1964B** in a total volume of 150 μL at 25 °C in 96-well polypropylene plates (Fisher Scientific, Pittsburgh, PA). Each well contained 20 μg protein while the concentrations of the radioligand ranged from 0.20 nM to 10.00 nM. Reactions were terminated by the addition of 100 μL of Tris-HCl buffer at 4 °C, then samples were harvested and filtered rapidly using a 96-well glass fiber filtration plate (Millipore, Billerica, MA) presoaked with 100 μL Tris-HCl assay buffer for 1 hour. Each filter was washed with 5 × 200 μL Tris-HCl buffer then transferred to a scintillation vial with 2 mL of scintillation fluid and counted on a Wallac 1450 MicroBeta TriLux liquid scintillation counter (Perkin Elmer, Boston, MA). The equilibrium dissociation constant (K_d) and maximum number of binding sites (B_{max}) were determined by nonlinear regression analysis of one-site saturation binding model using GraphPad Prism 5.0 (GraphPad Software, Inc., San Diego, CA).

For competitive binding assays, rat striatum homogenates P20 (4 μg protein) were incubated with [^{3}H]**TZ1964B** and each test compound in a total volume of 150 μL in 96 well plates for 60 min at 25 °C. The final concentration of the radioligand in each assay was 2 nM. Concentrations of test compounds ranging from 0.03 nM to 10 μM were added to provide inhibition curves. After incubation, samples were washed 5 times, bound radioactivity counted and analyzed by nonlinear regression using one-site competitive binding model using GraphPad Prism 5.0 (GraphPad Software, Inc., San Diego, CA).

In all the binding assays, the nonspecific binding of the radioligand was obtained in the presence of 10 μM of MP-10. Counts were normalized to mg protein in the sample. Three independent experiments were performed, the results are reported as mean ± standard deviation.

2.5 *In vitro* autoradiography in rat brain slices

Rats were euthanized, and the whole brain was immediately removed, then were snap frozen over dry ice. Horizontal sections (20 - 30 μm) were cut with a Microm cryostat (Microm HM 550; Microm International, Walldorf, Germany) and mounted on Superfrost Plus glass slides (Fisher Scientific, Pittsburgh, PA). All the sections were stored in −20 °C for no more than 1 month. The *in vitro* autoradiography was performed as previously reported (Xu et al., 2010). The sections were thawed and dried for 15 min at room temperature, and pre-incubated for 15 min in Tris-HCl buffer. The brain slices were then incubated for 60 min with [^{3}H]**TZ1964B** in different concentrations (0.38 - 12 nM) at room temperature. Nonspecific binding was determined from samples that contained additional 10 μM of

MP-10. To explore the regional distribution of PDE10A in the brain, sagittal rat brain sections, including striatum, frontal cortex, hippocampus, thalamus, globus pallidus, nucleus accumbens, substantia nigra, and cerebellum, were prepared and incubated with 3 nM [^{3}H]**TZ1964B** in the presence or absence of 10 μM of MP-10. Following the incubation, all sections received two rinses of 5 min each in ice-cold assay buffers and one quick rinse in ice-cold water. The sections were air-dried overnight and then exposed to the screen (Hyperfilm MP; Amersham-GE Healthcare, Piscataway, NJ) in an imaging cassette (Fuji Photo Film Co., Tokyo, Japan) for 4 weeks at room temperature. The film was then developed with a Kodak X-OMAT 2000A processor (Kodak, Tokyo, Japan). The optical density of images were analyzed by Image J (NIH, Bethesda, MD). The equilibrium dissociation constant K_d of ligand binding were calculated by nonlinear regression analysis of one-site saturation binding model using GraphPad Prism 5.0 (GraphPad Software, Inc., San Diego, CA).

2.6 *Ex vivo* autoradiography in the rat brain

Rats (n = 2) were anesthetized with 2-3% isoflurane/oxygen, and were injected with [^{11}C]**TZ1964B** (~ 74 MBq) via the tail vein. At 30 min post injection, rats were euthanized and the whole brains were dissected. Intact brains were flash frozen in dry ice, pre-cooled in isopentane and stored on dry ice. Horizontal sections (100 μm) were cut with a Microm cryostat and mounted on superfrost plus glass slides (Fisher Scientific, Pittsburgh, PA). Frozen slides were instantly exposed the film in an imaging cassette BAS- TR2025 (Fuji Photo Film, Tokyo, Japan) for 12 h in −20° C at dark. The distribution of radioactivity was visualized by a Fuji Bio-Imaging Analyzer FLA-7000 (Fuji Photo Film, Tokyo, Japan). Photo-stimulated luminescence (PSL) from the striatum and cerebellum were quantified using Multi Gauge v3.0 software (Fuji Photo Film, Tokyo, Japan). Data were background-corrected and expressed as photo-stimulated luminescence signals per square millimeter (PSL/mm^2).

2.7 *In vivo* microPET studies in NHPs

2.7.1 Subjects—PET imaging was carried out on two adult male cynomolgus monkeys. Subject A underwent 4 baseline scans, a series of scans for blocking studies using various doses of MP-10 (0.05, 0.10, 0.25, 0.50, 1.00, 1.50, and 2.00 mg/kg), and a scan for the displacement study (MP-10, dose of 2.00 mg/kg). Subject B underwent two baseline scans. The data represented the results of 6 baseline and 7 blocking experiments. Fasted animals were immobilized with ketamine (10 mg/kg, intramuscular) and anesthetized with 1.5–2.5% isoflurane via an endotracheal tube. A water-soluble ophthalmic ointment was placed in the eyes. Vital signs were monitored every 5 min, and the temperature was kept constant at ~37 °C with heated water blankets. An intravenous perfusion line permitted hydration and injection of the radiotracer.

2.7.2 PET data acquisition—A MicroPET Focus 220 scanner (Concorde/CTI/Siemens Microsystems, Knoxville, TN) was used for the imaging studies of [^{11}C]**TZ1964B** in the brains of nonhuman primates. A 10 min transmission scan was performed to check the positioning of the brain within the scanner; this was followed by a 45 min transmission scan for attenuation correction. Subsequently, a 120 min dynamic (3× 1-min frames, 4× 2-min

frames, 3× 3-min frames, and 20× 5-min frames) PET scan were acquired after intravenous injection of 185 - 259 MBq of [^{11}C]**TZ1964B**. Blocking experiments were conducted using escalating doses (0.05, 0.10, 0.25, 0.50, 1.00, 1.50 and 2.00 mg/kg) of MP-10 administered intravenously 5 min prior to the tracer injection. Displacement studies were conducted in subject A by administering MP-10 intravenously at dose of 2.00 mg/kg, 20 min post tracer injection.

2.7.3 PET images processing—Emission scans were corrected using individual attenuation, random correction and model-based scatter correction and reconstructed using filtered back projection as described previously (Miller et al., 1989). PET image reconstructed resolution was < 2.00 mm full width half maximum for all 3 dimensions at the center of the field of view. The monkey's magnetization-prepared rapid gradient echo (MP-RAGE) MR image and the summed PET images were co-registered using Automated Image Registration (AIR) (Woods et al., 1993). For quality control of this co-registration process, the co-registered PET and MRI were superimposed using Analyze 10.0 (AnalyzeDirect, Overland Park, KS) and any misalignments could be detected by misposition of brain edges on both images. For quantitative analyses, three-dimensional regions of interest (ROI) for cerebellum (583 voxels, the voxel size is 1.858 mm × 1.858 mm × 0.796 mm = 2.75 μL), striatum (695 voxels), frontal cortex (263 voxels), occipital cortex (254 voxels), temporal cortex (335 voxels), white matter (257 voxels) and hippocampus (68 voxels) were identified on the MRI and then transformed into baseline PET space using the co-registration transformation matrix. The ROIs once identified on a baseline scan were kept fixed for all subsequent studies on the same animal. These ROIs then were used to extract time activity curves from the dynamic PET images. Radioactivity measures were standardized to the body weight and the dose of radioactivity injected to yield standardized uptake value (SUV). To minimize noise signal in the presentation time tissue-activity curve (TAC) data have been smoothed by “Adjacent Averaging” using the OriginLab 9.1 program (OriginLab Corporation, Northampton, MA), while tracer kinetics analysis was based on original data without smoothing. All image analysis was carried out by investigators blinded to the blocking pretreatment.

2.7.4 Reference based tracer kinetic analysis—Quantification of specific uptake was compared with two tracer kinetic methods: Logan Reference (LoganREF) model (Innis et al., 2007; Logan et al., 1996; Logan et al., 1990) (**Figure S1**) and simplified reference tissue model (SRTM) (Gunn et al., 1997; Innis et al., 2007; Lammertsma and Hume, 1996) (**Figure S2**). Using the LoganREF model, the volume of distribution ratio (DVR) was estimated in each ROI using a MATLAB (Mathworks Inc., Natick, MA) implementation of these tracer kinetic methods as previously published (Logan et al., 1990). This enabled calculation of the binding potential (non-displaceable): BP_{ND} = DVR-1, which is proportional to the ratio B_{max}/K_d for each region of interest with fixed k_2’ value 0.10 min^{-1} (Van Laere et al., 2013b) and C_{ROI} values collected from the PET scans. BP_{ND} and R_1, k_2 values were also derived from the application of SRTM model. The model fitting was processed as previously published (Lammertsma and Hume, 1996; Watabe et al., 1996) with C_R (reference region tracer radioactive concentration) and C_T (target region tracer radioactive concentration) values derived from microPET collections. Percentage test–retest

variability (TRV) was calculated as the mean percentage between the absolute difference between test and retest and average test and retest values, $100\times|\ BP_{ND\text{-}test} - BP_{ND\text{-}retest}\ |/((\ BP_{ND\text{-}test} + BP_{ND\text{-}retest})/2)$. The coefficient of variation (CV = 100× standard deviation/mean BP_{ND}) is a measure of dispersion and often referred to as the relative standard deviation.

The regional target occupancy (Occ) following pretreatment with MP-10 was calculated directly as the relative change in striatal BP_{ND} using both LoganREF and SRTM; and it refers to the percentage of the enzyme PDE10A binding sites bound by the drug molecule (MP-10). The occupancy values were averaged across the striatal regions (putamen and caudate) to estimate the occupancy percentage. In addition, the occupancy values at baseline and after MP-10 pre-treatment were also analyzed using the occupancy plot (Suhara et al., 2003) to provide alternative estimates of the reduction of the specific signal.

3. Results

3.1 Radiochemical synthesis

The chemical structures of [^{3}H]**TZ1964B** and [^{11}C]**TZ1964B** are shown in **Figure 1**. The specific activity of [^{3}H]**TZ1964B** was 3145 MBq/μmol. [^{11}C] **TZ1964B** was obtained in high specific activity > 318.2 GBq/μmol (decay corrected to end of bombardment), with radiochemical yield 20 - 30% (decay corrected to end of bombardment,) and radiochemical purity >99%.

3.2 *In vitro* binding assays in rat brain homogenates

As an initial step, a kinetic binding characteristic of [^{3}H]**TZ1964B** binding to the PDE10A in rat striatum homogenates P20 was investigated. Both the association and dissociation time courses were shown in **Figure 2A&B**. After about 10 min at room temperature, > 95% of max specific [^{3}H]**TZ1964B** binding was achieved (K_{on} = 0.33 ± 0.13 $nM^{-1}\cdot min^{-1}$). The dissociation rate constant K_{off} of [^{3}H]**TZ1964B** binding was 0.41 ± 0.079 min^{-1}. Direct saturation binding studies were carried out using [^{3}H]**TZ1964B** with rat striatum homogenates P20. A single site binding was observed with K_d = 1.25 ± 0.20 nM and B_{max} = 8216 ± 400.60 fmol/mg protein (**Figure 2C&D**). A series of σ_1 receptor, σ_2 receptor, vesicular monoamine transporter 2 (VMAT2), vesicular acetylcholine transporter (VAChT), dopaminergic, serotonergic, or PDE1 specific ligands, and known PDE10A inhibitors were tested to characterize the pharmacological profile of [^{3}H]**TZ1964B** (Chemical structures shown in **Figure S3**). The K_i values for inhibiting [^{3}H]**TZ1964B** binding to PDE10A were obtained by competitive binding assays (**Table 1**). Specific PDE10A inhibitors displaced [^{3}H]**TZ1964B** binding in rat striatum with variable K_i values ranging from 0.015 nM to 251.4 nM (**Table 1, Figure 3**). No inhibition of the [^{3}H]**TZ1964B** binding to PDE10A was observed in the competitive binding studies using PDE1, σ_1 receptor, σ_2 receptor, VAChT, dopaminergic, and serotonergic ligands.

3.3 *In vitro* autoradiography in rat brain slices

To confirm the selectivity of [^{3}H]**TZ1964B** in different brain regions, *in vitro* autoradiography studies were performed using rat brain slices. As shown in **Figure 4A&B**,

[^{3}H]**TZ1964B** clearly accumulated in the striatum. The addition of 10 μM of MP-10 dramatically reduced the binding of [^{3}H]**TZ1964B** in the striatum. High radiotracer uptake also was found in globus pallidus, nucleus accumbens, and substantia nigra. Thalamus, cerebellum and frontal cortex showed trace to low level of [^{3}H]**TZ1964B** accumulation.

The specific uptake of [^{3}H]**TZ1964B** in rat striatum was 5.50-7.50-fold higher than that in cerebellum (**Figure 4C**, the ratio varied due to different concentrations of [^{3}H]**TZ1964B**). The saturation binding curve was shown in **Figure 4D**. [^{3}H]**TZ1964B** bound to the striatum in rat brain slices with a K_d value of 4.10 ± 1.74 nM.

3.4 *Ex vivo* autoradiography in the rat brain

Ex vivo autoradiography using [^{11}C]**TZ1964B** confirmed that the radiotracer clearly labelled the PDE10A sitesin rat striatum with high selectivity, whereas rare accumulation was observed in the cerebellum (**Figure 4E & F**). The uptake of [^{11}C]**TZ1964B** in rat striatum was ~6-fold higher than that in the cerebellum.

3.5 *In vivo* microPET studies in NHPs

The summed PET images from 0 to 120 min, showing the regional distribution of [^{11}C]**TZ1964B** at baseline, revealed [^{11}C]**TZ1964B** retention in striatum (**Figure 5A**). The selective PDE10A inhibitor MP-10, at a dose of 2.0 mg/kg, reduced significantly the striatal uptake of [^{11}C]**TZ1964B**, which confirmed the target specificity of [^{11}C]**TZ1964B** for PDE10A. The average SUV curve (6 baseline scans in 2 NHPs, **Figure 5B**) showed consistently high accumulation of the radiotracer in the striatum, and fast wash-out in the cerebellum. The striatum to cerebellum ratio was ~5.50 at 90 min post-injection. Using the cerebellum as the reference region, the graphical analysis by LoganREF model showed the uptake of [^{11}C]**TZ1964B** in the striatum is much higher than other brain regions, including cortex, hippocampus and white matter (**Figure 5C**).

For a 120-min acquisition time of baseline scans, the BP_{ND} calculated with the LoganREF model for the striatum was 3.96 ± 0.17 (n = 6, **Table 2**), using the cerebellum as the reference region. The BP_{ND} value using the SRTM for the striatum was 4.64 ± 0.47 (n = 6, **Table 2**). The examination of test-retest reproducibility and variability was presented in **Table 3**. The first two scans of subject A and B were used. The average percent changes between test and retest BP_{ND} values in the striatum were 4.80% for LoganREF model and 13.80% for SRTM. The test-retest variability (TRV) were 4.62% for LoganREF model and 13.10% for SRTM.

As shown in **Figure 6A**, MP-10 dose-dependently blocked the [^{11}C]**TZ1964B** uptake in the striatum. When pretreating with MP-10 at dose of 0.25 mg/kg, the striatal BP_{ND} was reduced by 26.69% and 17.76%, calculated by LoganREF and SRTM, respectively (**Figure 6A, Table 4**). Pretreatment using MP-10 at dose of 2.00 mg/kg decreased the striatal BP_{ND} by 89.29% (LoganREF) and 85.87% (SRTM) (**Figure 6A, Table 4**). MP-10 (2.00 mg/kg) administration 20 min post injection of [^{11}C]**TZ1964B** displaced radiotracer from striatum (**Figure 6B**). On the other hand, cerebellar uptake was not affected by either pretreatment

(blocking) or post-treatment (displacement) studies, validating the use of cerebellum as a suitable reference region.

The data acquired from NHPs pretreated with different doses of MP-10 was used to determine the target occupancy after administration of different doses of MP-10 and to estimate the *in vivo* affinity. The BP_{ND} values (both from LoganREF and SRTM) for occupancy studies are shown in **Table 4**. The reduction of BP_{ND} corresponds with increasing dose of pretreatment with MP-10. MP-10 pretreatment doses of 0.05, 0.10, 0.25, 0.50, 1.00, 1.50 and 2.00 mg/kg produced occupancy levels of 5.01%, 4.06%, 26.26%, 79.09%, 77.14%, 89.17% and 89.23% determined by LoganREF (BP_{ND}) or 18.07%, 17.19%, 22.32%, 73.37%, 81.63%, 80.00% and 86.65% determined by SRTM (BP_{ND}). Scatter plot of BP_{ND} in the striatum with SRTM versus BP_{ND} LoganREF modeling showed good correlation ($r^2 = 0.94$), including data from both baseline and different doses of MP-10 pretreatments (**Figure 7A**). The fitted ED_{50} is 0.31 ± 0.09 mg/kg (LoganREF) and 0.45 ± 0.17 mg/kg (SRTM) (**Figure 7B**).

4. Discussion

Recently, several potent radiotracers targeting PDE10A have been developed and validated *in vivo* by different groups (Barret et al., 2014; Barret, 2012; Celen et al., 2010; Celen et al., 2013; Harada et al., 2015; Hwang et al., 2014; Kehler et al., 2014; Van Laere et al., 2013a; Van Laere et al., 2013b), including another radiolabeled MP-10 analogue, [^{18}F]JNJ42259152. However, as found with MP-10, the possible influence of a brain-penetrating radioactive metabolite of [^{18}F]JNJ42259152 was reported (Celen et al., 2013; Van Laere et al., 2013b). To overcome the common radiolabeled metabolite problem, as reported, we radiosynthesized and preliminarily evaluated a series of new pyrazole group-containing analogues, with a methoxy group on the quinoline fragment (Li et al., 2013). **TZ1964B** displayed a favorable metabolic stability and was selected as the most promising candidate of PET ligands for PDE10A (Fan et al., 2014). Thus in the present study, [^{11}C]**TZ1964B** and its radiolabeled counterpart [^{3}H]**TZ1964B** were further investigated both *in vitro* and *in vivo*.

Saturation binding assays in rat striatum homogenates revealed that [^{3}H]**TZ1964B** has a nanomolar K_d value (1.25 nM), which was consistent with the value obtained from kinetic binding experiments (K_{off}/K_{on} = 1.24 nM). Moreover, obtained from kinetic binding studies, both of the association rate (K_{on}) and the dissociation rate (K_{off}) were fast, which indicated that the tracer [^{3}H]**TZ1964B** binds to the PDE10A binding site quickly, and that the binding is reversible (Hulme and Trevethick, 2010). A similar K_d value (4.10 ± 1.74 nM) in rat striatum was also observed in autoradiographic studies. The slight difference between homogenate binding assays and the brain slice autoradiography has been previously reported (Harada et al., 2015), which might be attributed to the purification of the target protein in the former study.

In competitive binding assays, [^{3}H]**TZ1964B** has little affinity for PDE1, σ_1, σ_2, VAChT, dopaminergic, or serotonergic receptors/proteins. Only PDE10A compounds reduced specific binding, confirming the specificity of [^{3}H]**TZ1964B** binding. Interestingly, among

those PDE10A compounds used in competitive binding assay, papavarine and its analogues (**9a** and **9c**) had comparably very large K_i values (>100 nM), while MP-10 and other 3 analogues (TZ1914B, TZ1982T, TZ19106B) had nanomalar K_i values. The different competitive binding patterns of these two categories of PDA10A compounds could be explained by their different binding sites to PDE10A enzyme. According to the crystal structures, MP-10 binds to the "selectivity pocket" of PDE10A that is in proximity to the catalytic site of the enzyme, while papavarine and its analogues only binds to the hydrophobic clamp and exo-binding region (Chappie et al., 2012). Furthermore, the chemical structure of MP-10 analogue **TZ1914B** shows that the fluorine group in the quinoline fragment locates at the fourth position, instead of at the third position as shown in other 2 MP-10 analogues. The group at the fourth position is close to the M-loop of PDE10A (Chappie et al., 2012), and may be contributed to a comparably low competitive binding affinity of **TZ1914B**.

Besides nanomolar binding affinity, a high target-to-reference ratio of the radiotracer uptake is required for PET imaging. Therefore, selecting a proper reference region is critical for both *in vitro* and *in vivo* validation of novel PET radiotracers. Although the PDE10A distribution in the brain is mainly restricted to the striatum, other brain regions including cortex, thalamus and cerebellum show trace to low levels of PDE10A expression (Seeger et al., 2003). The cerebellum has been used as the reference tissue for the assessment of regional binding potentials for PDE10A radiotracers (Barret, 2012; Kehler et al.,2014; Lin et al., 2015). The frontal cortex and the thalamus were also used as the reference region in human or NHP PET studies (Hwang et al., 2014; Van Laere et al., 2013b). To validate a suitable brain region as the reference for our new tracer, *in vitro* distribution of [^{3}H]**TZ1964B** in the brain was examined by *in vitro* autoradiography. The cerebellum and frontal cortex showed similar low levels of radiotracer uptake, with an even lower level in the thalamus. However, there was no difference in the specific binding in the above three regions. Moreover, our initial microPET imaging of [^{11}C]**TZ1964B** in NHP showed consistently low tracer accumulation in both the cerebellum and the thalamus, with a slightly high uptake in the frontal cortex.

Accordingly, both the cerebellum and the thalamus may serve as the candidate of reference regions for [^{11}C]**TZ1964B** PET imaging. In the current study, the cerebellum was chosen for further characterization of radiolabelled **TZ1964B** both *in vitro* and *in vivo*, as the striatum-to-cerebellum ratio is a widely used index for the specificity of PDE10A tracers, permitting comparisons with others radiotracers. The lack of alteration of cerebellar uptake of [^{3}H]**TZ1964B** and [^{11}C]**TZ1964B** by blocking or pretreatment with high dose of MP-10 further confirms the suitability of this area as an appropriate reference region for these analyses. The specific uptake of [^{3}H]**TZ1964B** and [^{11}C]**TZ1964B** in the rat striatum was 5.50-7.50 fold higher than that in the cerebellum (the reference region), found by *in vitro* and *ex vivo* autoradiography, respectively. The striatum-to-cerebellum ratio approximated that from a previous biodistribution study (the ratio was 6.00 at 60 min post-injection) (Fan et al., 2014). Nevertheless, the use of cerebellum as the reference region needs to be confirmed further by arterial blood input analysis in the future.

The *in vitro* data justified investigation of characterization of the *in vivo* binding properties of [^{11}C]**TZ1964B** in NHPs. Baseline scans demonstrated that [^{11}C]**TZ1964B** consistently and selectively accumulated in the NHP striatum. The average striatum to cerebellum (target to reference) ratio after steady state (~5.50) was close to that observed in *in vitro* and *ex vivo* autoradiographic studies. We applied the LoganREF model and the SRTM to determine the binding potential BP_{ND} values with the cerebellum as the reference region. The average striatal BP_{ND} value was 3.96 (by LoganREF model), and 4.64 (by SRTM). The BP_{ND} values using these two models correlated well, although LoganREF model gave lower values, as previously reported in PET imaging analysis of several C-11 labeled radiotracers (Yamasaki et al., 2014; Zanderigo et al., 2013). Moreover, the reproducibility and reliability of the striatal BP_{ND} values, calculated by both LoganREF model and SRTM, was evidenced by the low test-retest variability and the low coefficient of variance. The good correlation and the high reliability of these two modelling methods indicated both LoganREF model and SRTM could be applied for PET data analysis of [^{11}C]**TZ1964B** scans in the brain.

The *in vivo* binding specificity of [^{11}C]**TZ1964B** was investigated by pretreatment with different doses of MP-10. The regional tissue time-activity curves revealed that the uptake of [^{11}C]**TZ1964B** in the striatum, but not in the cerebellum, was reduced following MP-10 pretreatment. In the displacement study, following the MP-10 administration, the uptake of [^{11}C]**TZ1964B** in the striatum was reduced to the similar level of the cerebellum uptake at the end of PET scan. Along with the *in vitro* binding assay data, these data demonstrate that[^{11}C]**TZ1964B** binds specifically to PDE10A, and that the binding is reversible. Furthermore, intravenous injection of MP-10 occupied PDE10A specific striatal binding sites in NHPs. The MP-10 dose of 0.31 ± 0.09 mg/kg (LoganREF) / 0.45 ± 0.17 mg/kg (SRTM) produced about 50% PDE10A occupancy in the striatum. These results provided an example of estimating PDE10A occupancy, and generated key information on the pharmacokinetic-pharmacodynamics relationship of MP-10 (Borroni et al., 2013). The estimated *in vivo* binding affinity for MP-10 agreed well with the ED50 value measured by [^{11}C]MP-10 (0.30 mg/kg) (Plisson et al., 2011), which further supports the suitability of [^{11}C]**TZ1964B** in quantifying the *in vivo* binding sites for PDE10A and evaluating the target occupancy of new-synthesized PDE10A inhibitors.

In conclusion, our results indicate that [^{11}C]**TZ1964B** has a nanomolar affinity and specificity to PDE10A, has high selectivity for the targeted brain region (striatum), and possesses good characteristics for the *in vivo* quantification of the PDE10A levels. Furthermore, [^{11}C]**TZ1964B** has great potential for evaluation of target occupancy of drugs targeting PDE10A. Therefore, [^{11}C]**TZ1964B** could serve as a suitable candidate for *in vivo* detecting PDE10A levels in human brain.

Supplementary Material

Refer to Web version on PubMed Central for supplementary material.

Acknowledgements

This work was supported by the National Institute of Mental Health (NIMH) of the National Institutes of Health (No. MH092797) and National Institute of Neurological Disorders and Stroke (NINDS, No. NS075527,

NS061025). The Cyclotron Facility of Washington University provided the [^{11}C]methyl iodide for radiolabeling studies. We would like to thank Emily William, Christina Zukas, Darryl Craig and John Hood for the technique support in NHP microPET studies, Dr. Tom Ellenberger for providing the high-speed centrifuge, Lynne Jones and Adam Rosenberg for manuscript revision, and Jinbin Xu for his technical assistance in the binding assay studies.

Abbreviations

AIR	automated Image Registration
BP_{ND}	binding potential (non-displaceable)
CNS	central nervous system
C_R	reference region tracer radioactivity concentration
C_T	target region tracer radioactivity concentration
DMF	*N*,*N*-dimethylformamide
DVR	volume of distribution ratio
LoganREF	Logan Reference
MP-RAGE	magnetization-prepared rapid gradient echo
MSN	medium spiny neuron
NHPs	nonhuman primates
Occ	target occupancy
PDE10A	phosphodiesterase 10A
PSL	photo-stimulated luminescence
ROI	region of interest
SD	Sprague-Dawley
SRTM	simplified reference tissue model
SUV	standardized uptake value
TRV	percentage test–retest variability
VAChT	vesicular acetylcholine transporter
VMAT2	vesicular monoamine transporter 2

References

Barret O, Thomae D, Tavares A, Alagille D, Papin C, Waterhouse R, McCarthy T, Jennings D, Marek K, Russell D, Seibyl J, Tamagnan G. In Vivo Assessment and Dosimetry of 2 Novel PDE10A PET Radiotracers in Humans: ^{18}F-MNI-659 and ^{18}F-MNI-654. J Nucl Med. 2014; 55:1297–1304. [PubMed: 24898025]

Barret OT, D. Alagille D, Lee H, Papin C, Baldwin R, Jennings D, Marek K, Seibyl J, Tamagnan G. First in vivo assessment of two PDE10 tracers [^{18}F]MNI654 and [^{18}F]MNI659. J. Nucl. Med. 2012; 53:361.

Borroni E, Zhou Y, Ostrowitzki S, Alberati D, Kumar A, Hainzl D, Hartung T, Hilton J, Dannals RF, Wong DF. Pre-clinical characterization of [C-11]R05013853 as a novel radiotracer for imaging of the glycine transporter type 1 by positron emission tomography. Neuroimage. 2013; 75:291–300. [PubMed: 22178811]

Celen S, Koole M, De Angelis M, Sannen I, Chitneni SK, Alcazar J, Dedeurwaerdere S, Moechars D, Schmidt M, Verbruggen A, Langlois X, Van Laere K, Andres JI, Bormans G. Preclinical Evaluation of F-18-JNJ41510417 as a Radioligand for PET Imaging of Phosphodiesterase-10A in the Brain. Journal of Nuclear Medicine. 2010; 51:1584–1591. [PubMed: 20847170]

Celen S, Koole M, Ooms M, De Angelis M, Sannen I, Cornelis J, Alcazar J, Schmidt M, Verbruggen A, Langlois X, Van Laere K, Andres JI, Bormans G. Preclinical evaluation of [^{18}F]JNJ42259152 as a PET tracer for PDE10A. Neuroimage. 2013; 82:13–22. [PubMed: 23664955]

Chappie TA, Helal CJ, Hou XJ. Current Landscape of Phosphodiesterase 10A (PDE10A) Inhibition. Journal of Medicinal Chemistry. 2012; 55:7299–7331. [PubMed: 22834877]

Fan J, Zhang X, Li J, Jin H, Padakanti PK, Jones LA, Flores HP, Su Y, Perlmutter JS, Tu Z. Radiosyntheses and in vivo evaluation of carbon-11 PET tracers for PDE10A in the brain of rodent and nonhuman primate. Bioorg Med Chem. 2014; 22:2648–2654. [PubMed: 24721831]

Gunn RN, Lammertsma AA, Hume SP, Cunningham VJ. Parametric imaging of ligand-receptor binding in PET using a simplified reference region model. Neuroimage. 1997; 6:279–287. [PubMed: 9417971]

Harada A, Suzuki K, Miura S, Hasui T, Kamiguchi N, Ishii T, Taniguchi T, Kuroita T, Takano A, Stepanov V, Halldin C, Kimura H. Characterization of the binding properties of T-773 as a PET radioligand for phosphodiesterase 10A. Nucl Med Biol. 2015; 42:146–154. [PubMed: 25451212]

Hulme EC, Trevethick MA. Ligand binding assays at equilibrium: validation and interpretation. British Journal of Pharmacology. 2010; 161:1219–1237. [PubMed: 20132208]

Hwang DR, Hu E, Rumfelt S, Easwaramoorthy B, Castrillon J, Davis C, Allen JR, Chen H, Treanor J, Abi-Dargham A, Slifstein M. Initial characterization of a PDE10A selective positron emission tomography tracer [^{11}C]AMG 7980 in non-human primates. Nucl Med Biol. 2014; 41:343–349. [PubMed: 24607437]

Innis RB, Cunningham VJ, Delforge J, Fujita M, Giedde A, Gunn RN, Holden J, Houle S, Huang SC, Ichise M, Lida H, Ito H, Kimura Y, Koeppe RA, Knudsen GM, Knuuti J, Lammertsma AA, Laruelle M, Logan J, Maguire RP, Mintun MA, Morris ED, Parsey R, Price JC, Slifstein M, Sossi V, Suhara T, Votaw JR, Wong DF, Carson RE. Consensus nomenclature for in vivo imaging of reversibly binding radioligands. Journal of Cerebral Blood Flow and Metabolism. 2007; 27:1533–1539. [PubMed: 17519979]

Kehler J, Kilburn JP, Estrada S, Christensen SR, Wall A, Thibblin A, Lubberink M, Bundgaard C, Brennum LT, Steiniger-Brach B, Christoffersen CT, Timmermann S, Kreilgaard M, Antoni G, Bang-Andersen B, Nielsen J. Discovery and Development of C-11-Lu AE92686 as a Radioligand for PET Imaging of Phosphodiesterase10A in the Brain. Journal of Nuclear Medicine. 2014; 55:1513–1518. [PubMed: 24994928]

Lammertsma AA, Hume SP. Simplified reference tissue model for PET receptor studies. Neuroimage. 1996; 4:153–158. [PubMed: 9345505]

Li JF, Jin HJ, Zhou HY, Rothfuss J, Tu ZD. Synthesis and in vitro biological evaluation of pyrazole group-containing analogues for PDE10A. Medchemcomm. 2013; 4:443–449. [PubMed: 23585921]

Lin SF, Labaree D, Chen MK, Holden D, Gallezot JD, Kapinos M, Teng JK, Najafzadeh S, Plisson C, Rabiner EA, Gunn RN, Carson RE, Huang Y. Further evaluation of [^{11}C]MP-10 as a radiotracer for phosphodiesterase 10A: PET imaging study in rhesus monkeys and brain tissue metabolite analysis. Synapse. 2015; 69:86–95. [PubMed: 25450608]

Logan J, Fowler JS, Volkow ND, Wang GJ, Ding YS, Alexoff DL. Distribution volume ratios without blood sampling from graphical analysis of PET data. Journal of Cerebral Blood Flow and Metabolism. 1996; 16:834–840. [PubMed: 8784228]

Logan J, Fowler JS, Volkow ND, Wolf AP, Dewey SL, Schlyer DJ, MacGregor RR, Hitzemann R, Bendriem B, Gatley SJ, et al. Graphical analysis of reversible radioligand binding from time-activity measurements applied to [N-11C-methyl]-(−)-cocaine PET studies in human subjects. J Cereb Blood Flow Metab. 1990; 10:740–747. [PubMed: 2384545]

Miller TR, Wallis JW, Wilson AD. Interactive reconstruction in single-photon tomography. Eur J Nucl Med. 1989; 15:189–193. [PubMed: 2787746]

Nishi A, Kuroiwa M, Shuto T. Mechanisms for the modulation of dopamine d(1) receptor signaling in striatal neurons. Front Neuroanat. 2011; 5:43. [PubMed: 21811441]

Plisson C, Salinas C, Weinzimmer D, Labaree D, Lin SF, Ding YS, Jakobsen S, Smith PW, Eiji K, Carson RE, Gunn RN, Rabiner EA. Radiosynthesis and in vivo evaluation of [^{11}C]MP-10 as a positron emission tomography radioligand for phosphodiesterase 10A. Nucl Med Biol. 2011; 38:875–884. [PubMed: 21843784]

Seeger TF, Bartlett B, Coskran TM, Culp JS, James LC, Krull DL, Lanfear J, Ryan AM, Schmidt CJ, Strick CA, Varghese AH, Williams RD, Wylie PG, Menniti FS. Immunohistochemical localization of PDE10A in the rat brain. Brain Res. 2003; 985:113–126. [PubMed: 12967715]

Soderling SH, Bayuga SJ, Beavo JA. Isolation and characterization of a dual-substrate phosphodiesterase gene family: PDE10A. Proc Natl Acad Sci U S A. 1999; 96:7071–7076. [PubMed: 10359840]

Strick, CAS.; C. J.; Menniti, FS. PDE10A: a striatum-enriched, dual-substrate phosphodiesterase.. In: Joseph, ABS.; H. F.; Miles, DH., editors. Cyclic Nucleotide Phosphodiesterases in Health and Disease. CRC Press; 2010. p. 237-254.

Suhara T, Takano A, Sudo Y, Ichimiya T, Inoue M, Yasuno F, Ikoma Y, Okubo Y. High levels of serotonin transporter occupancy with low-dose clomipramine in comparative occupancy study with fluvoxamine using positron emission tomography. Archives of General Psychiatry. 2003; 60:386–391. [PubMed: 12695316]

Tu Z, Fan J, Li S, Jones LA, Cui J, Padakanti PK, Xu J, Zeng D, Shoghi KI, Perlmutter JS, Mach RH. Radiosynthesis and in vivo evaluation of [^{11}C]MP-10 as a PET probe for imaging PDE10A in rodent and non-human primate brain. Bioorg Med Chem. 2011; 19:1666–1673. [PubMed: 21315609]

Tu Z, Xu J, Jones LA, Li S, Mach RH. Carbon-11 labeled papaverine as a PET tracer for imaging PDE10A: radiosynthesis, in vitro and in vivo evaluation. Nucl Med Biol. 2010; 37:509–516. [PubMed: 20447563]

Van Laere K, Ahmad RU, Hudyana H, Celen S, Dubois K, Schmidt ME, Bormans G, Koole M. Human biodistribution and dosimetry of ^{18}F-JNJ42259152, a radioligand for phosphodiesterase 10A imaging. Eur J Nucl Med Mol Imaging. 2013a; 40:254–261. [PubMed: 23160998]

Van Laere K, Ahmad RU, Hudyana H, Dubois K, Schmidt ME, Celen S, Bormans G, Koole M. Quantification of ^{18}F-JNJ-42259152, a novel phosphodiesterase 10A PET tracer: kinetic modeling and test-retest study in human brain. J Nucl Med. 2013b; 54:1285–1293. [PubMed: 23843566]

Watabe H, Itoh M, Cunningham V, Lammertsma AA, Bloomfield P, Mejia M, Fujiwara T, Jones AKP, Jones T, Nakamura T. Noninvasive quantification of rCBF using positron emission tomography. Journal of Cerebral Blood Flow and Metabolism. 1996; 16:311–319. [PubMed: 8594064]

Woods RP, Mazziotta JC, Cherry SR. MRI-PET registration with automated algorithm. J Comput Assist Tomogr. 1993; 17:536–546. [PubMed: 8331222]

Xie Z, Adamowicz WO, Eldred WD, Jakowski AB, Kleiman RJ, Morton DG, Stephenson DT, Strick CA, Williams RD, Menniti FS. Cellular and subcellular localization of PDE10A, a striatum-enriched phosphodiesterase. Neuroscience. 2006; 139:597–607. [PubMed: 16483723]

Xu J, Hassanzadeh B, Chu W, Tu Z, Jones LA, Luedtke RR, Perlmutter JS, Mintun MA, Mach RH. [^{3}H]4-(dimethylamino)-N-(4-(4-(2-methoxyphenyl)piperazin-1-yl) butyl)benzamide: a selective radioligand for dopamine D(3) receptors. II. Quantitative analysis of dopamine D(3) and D(2) receptor density ratio in the caudate-putamen. Synapse. 2010; 64:449–459. [PubMed: 20175227]

Yamasaki T, Maeda J, Fujinaga M, Nagai Y, Hatori A, Yui J, Xie L, Nengaki N, Zhang MR. PET brain kinetics studies of (11)C-ITMM and (11)C-ITDM,radioprobes for metabotropic glutamate receptor type 1, in a nonhuman primate. Am J Nucl Med Mol Imaging. 2014; 4:260–269. [PubMed: 24795840]

Zanderigo F, Ogden RT, Parsey RV. Reference region approaches in PET: a comparative study on multiple radioligands. J Cereb Blood Flow Metab. 2013; 33:888–897. [PubMed: 23423188]

Highlights

- [3H]**TZ1964B** has a high potency (K_d = 1.25 nM) and high target selectivity (~6-fold)
- [11C]**TZ1964B** has a high binding potential (3.96-4.64) and high binding specificity in the brain of nonhuman primate
- [11C]**TZ1964B** showed reversible binding property in the monkey striatum
- [11C]**TZ1964B** is a promising PET imaging tracer for assessing PDE10A in the brain

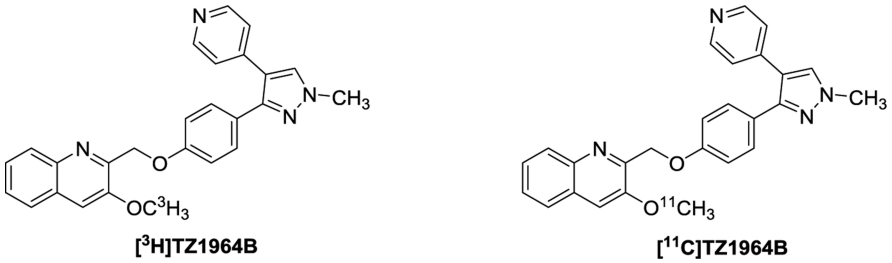

Figure 1.
Chemical Structures of [^{3}H]**TZ1964B** and [^{11}C]**TZ1964B**

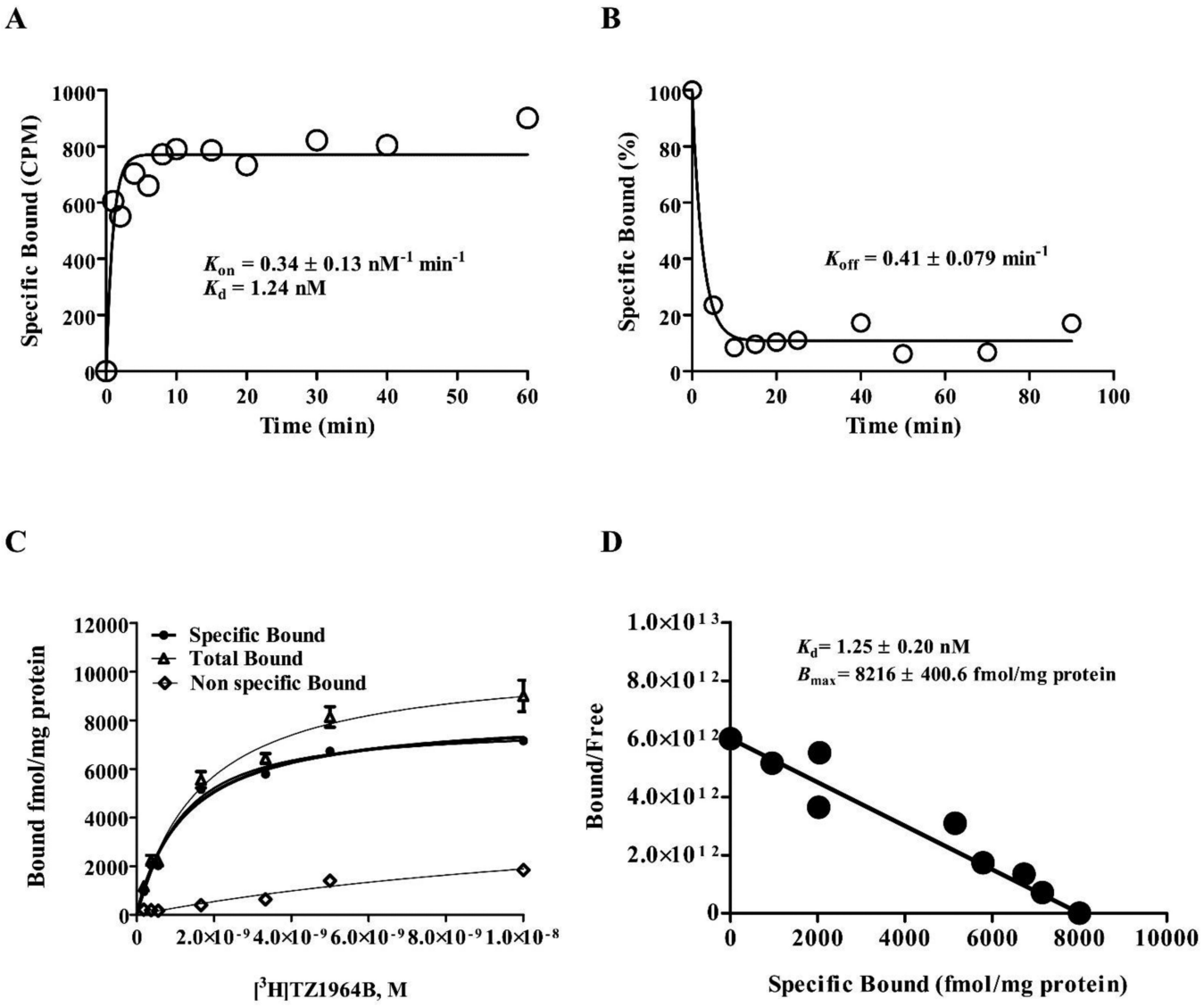

Figure 2.

Representative kinetic and saturation binding analysis of [^{3}H]**TZ1964B** to PDE10A in P20 fractions of rat striatum homogenates. (A, association experiment; B, dissociation experiment; C, saturation binding curve; D, Scatchard analysis.)

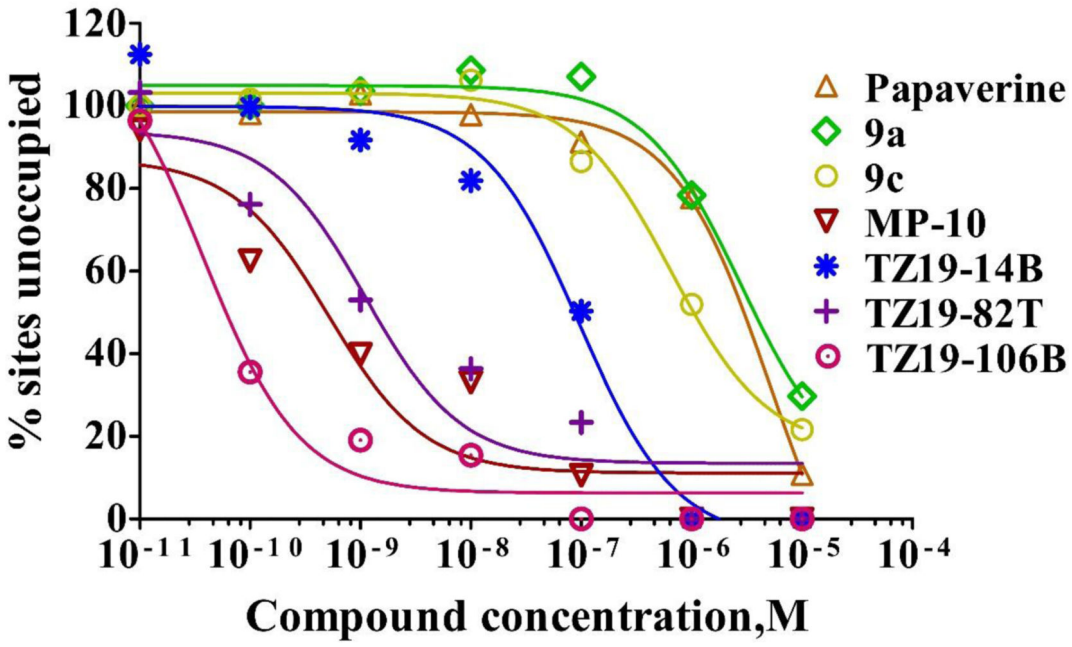

Figure 3.

Representative competitive binding analysis of the binding of [^{3}H]**TZ1964B** to PDE10A in P20 fractions of rat striatum homogenates.

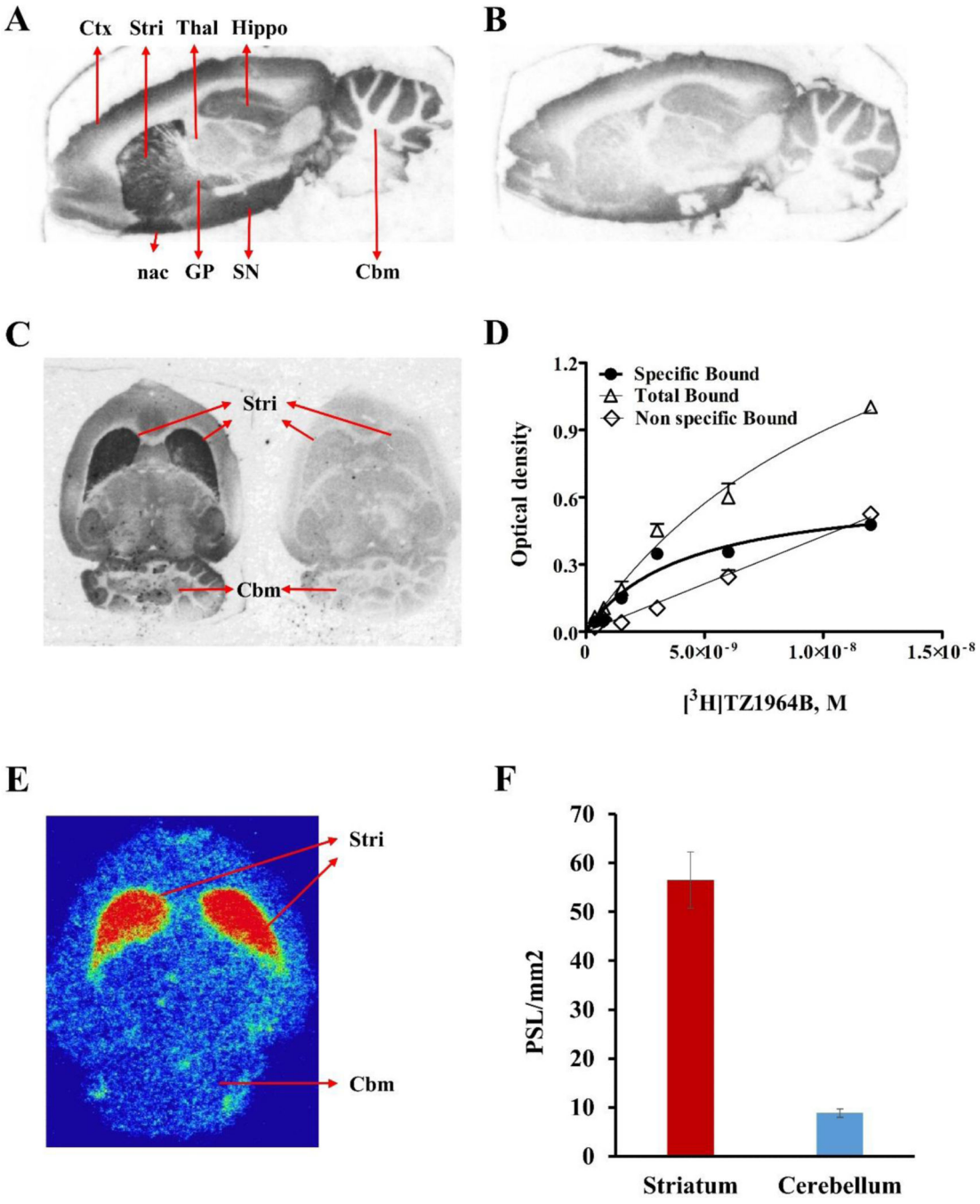

Figure 4.

In vitro and/or *ex vivo* binding specificity and brain distribution of [^{3}H]**TZ1964B** and [^{11}C]**TZ1964B** in rat brain. Representative images of *in vitro* autoradiography of [^{3}H]**TZ1964B** in rat brain showed high radiotracer uptake in striatum, globus pallidus, nucleus accumbens, and substantia nigra, which could be blocked by MP-10 (A, sagittal section; B, sagittal section with MP-10 blocking; C, horizontal section with and without MP-10 blocking; D. Saturation binding curve obtained from striatal uptake of [^{3}H]**TZ1964B**). Representative images of *ex vivo* autoradiography of [^{11}C]**TZ1964B** in rat

brain (E, horizontal section; F, Bar graph showing binding intensity.) confirmed the high radiotracer uptake in the striatum, but not in the cerebellum. PSL/mm^2, photo-stimulated luminescence signals per square millimeter.

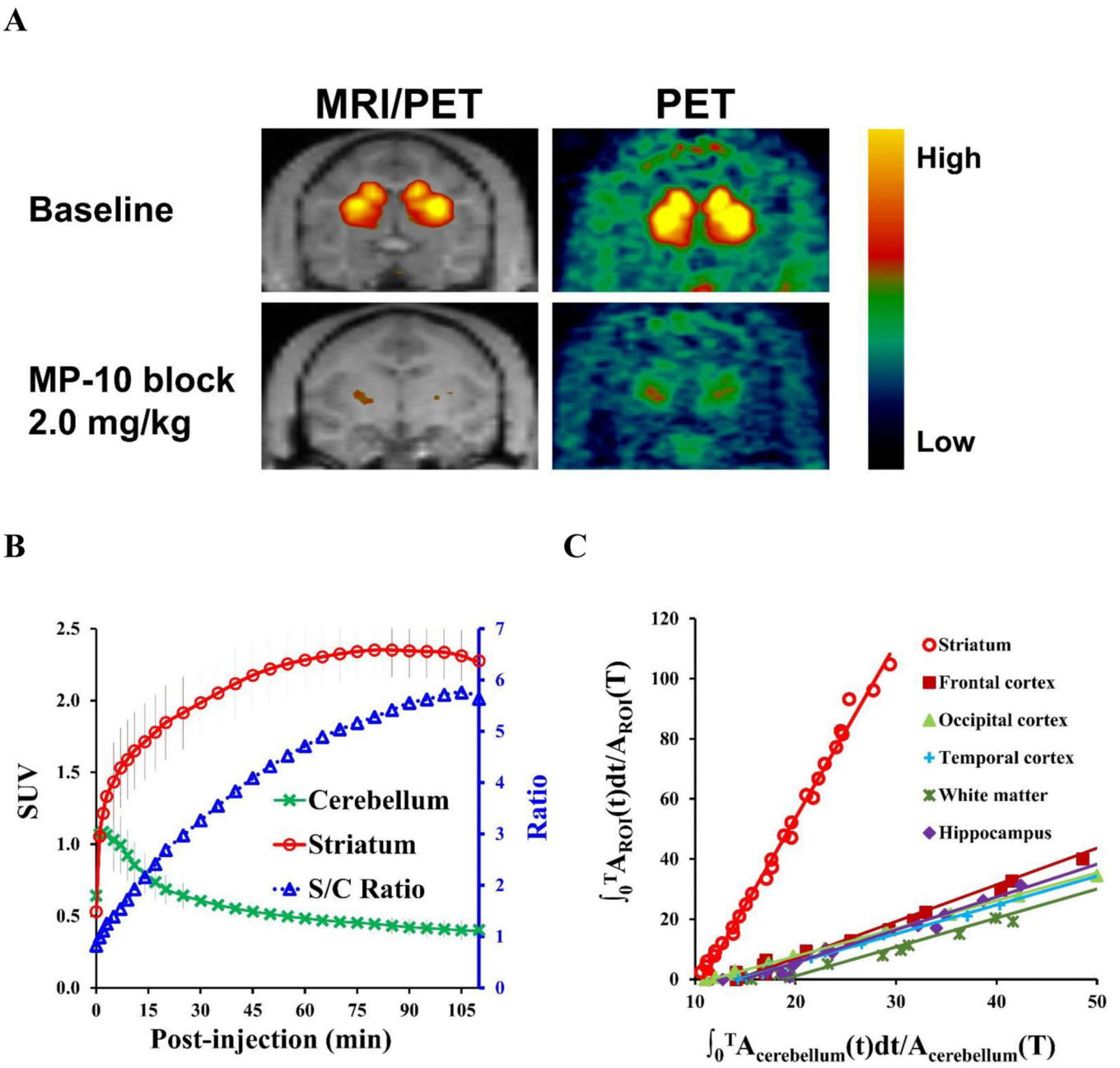

Figure 5.

In vivo binding specificity and brain distribution of [^{11}C]**TZ1964B** in non-human primates (NHPs). Representative PET and the co-registered MRI/PET images of [^{11}C]**TZ1964B** in NHPs (A, summed radioactivity from 0 to 120 min) and averaged SUV curves of striatum and cerebellum (n = 6, B) indicated the tracer consistently accumulated in the NHP striatum, which could be blocked by MP-10 pretreatment. The average striatum to cerebellum (target to reference) ratio near steady state was ~5.50. Graphical analysis by LoganREF model also revealed the striatum has much higher radiotracer uptake than other brain regions (C).

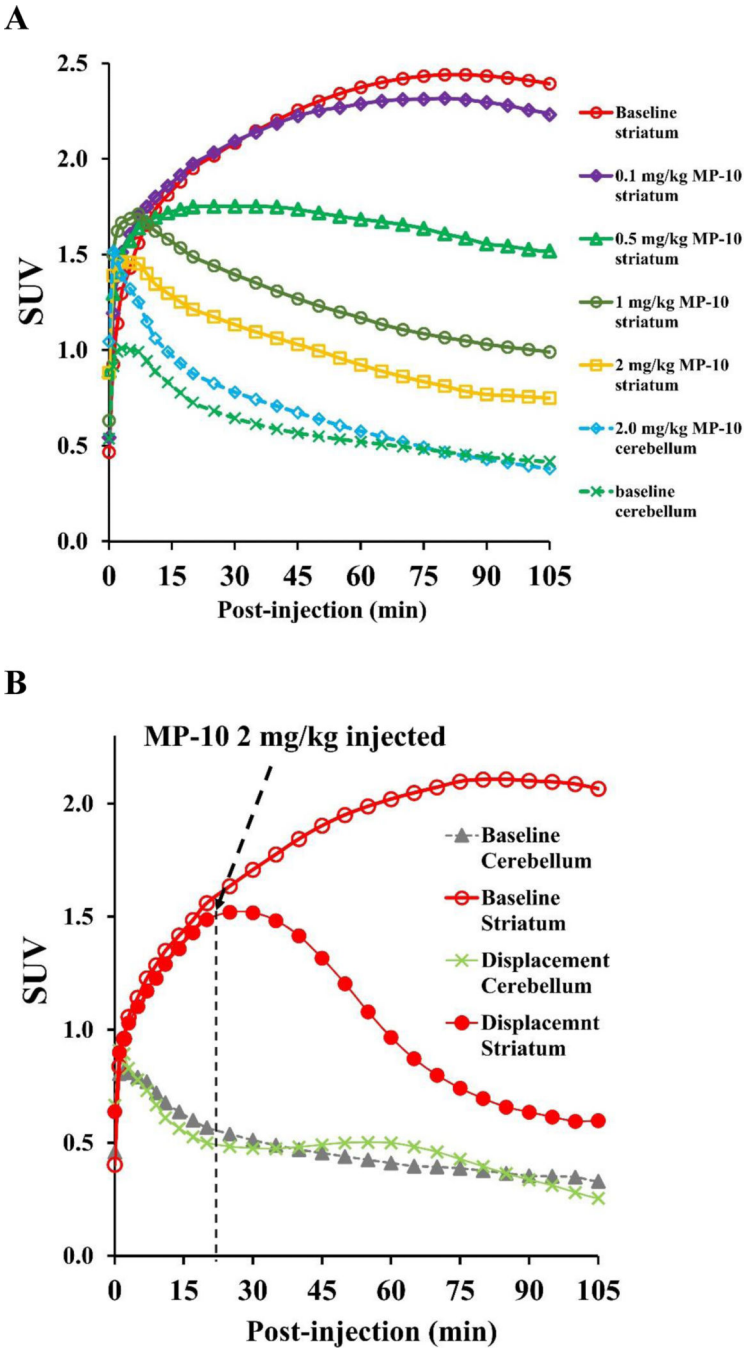

Figure 6.

Blocking and displacement study of [^{11}C]**TZ1964B** in NHPs. SUV curves showing the striatal uptake, but not the cerebellar uptake, of [^{11}C]**TZ1964B** was dose-dependently decreased by MP-10 pretreatment (A). The binding of [^{11}C]**TZ1964B** in NHP striatum was also reduced by MP-10 displacement (B), indicating a reversible tracer binding property.

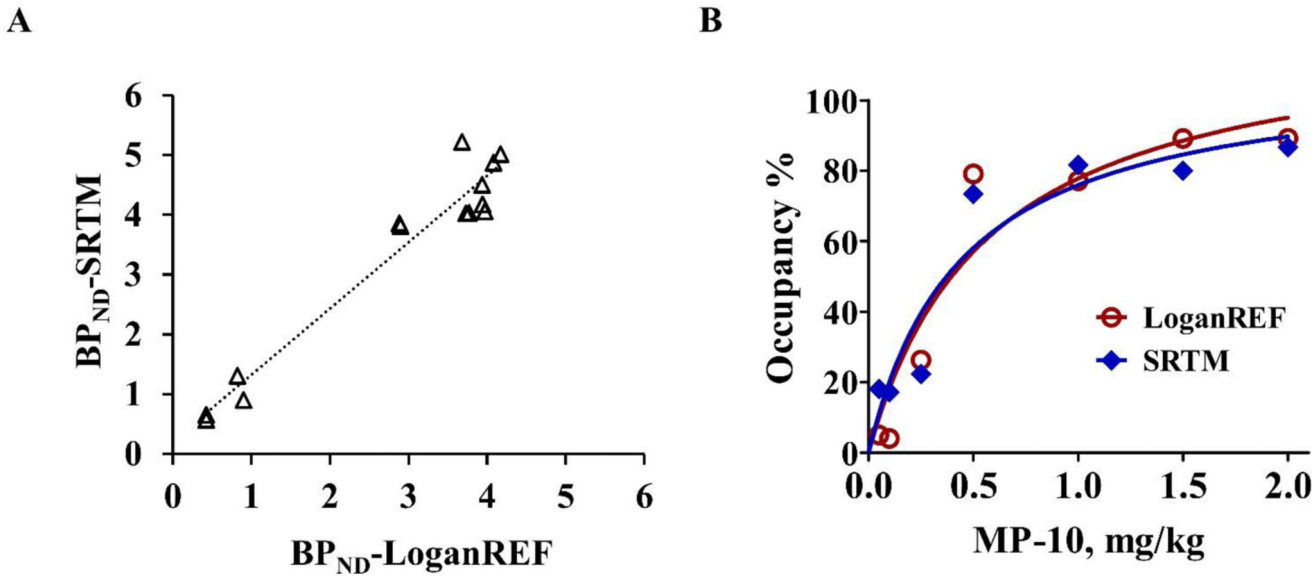

Figure 7.

MP-10 dose and PDE10A occupancy relationship. A. Scatter plot of BP_{ND} in the striatum with SRTM versus BP_{ND} LoganREF modeling showed good correlation. B. Target occupancy curves using LoganREF (red) and SRTM (blue) respectively. The fitted ED_{50} is 0.31 ± 0.09 mg/kg (LoganREF) and 0.45 ± 0.17 mg/kg (SRTM).

Table 1

Summary of the PDE10A binding affinity of a series compounds obtained from competitive binding study with [^{3}H]**TZ1964B** using P20 fractions of rat striatum homogenates

Drugs	Selectivity	K_i, nM
TZ19106B	PDE10A	0.015 ± 0.002
MP-10	PDE10A	0.20 ± 0.06
TZ1982T	PDE10A	0.42 ± 0.10
TZ1914B	PDE10A	36.89 ± 4.51
9c	PDE10A	251.40 ± 44.67
9a	PDE10A	>1000
Papaverine	PDE10A	>1000
Vinpocetine	PDE1	>1000
Pentazocine	Sigma 1	>1000
ISO-1	Sigma2	>1000
Ditolylguanidine (DTG)	Sigma 1/2	>1000
WAY-100135	5-HT1A	>1000
Haloperidol	D2	>1000
Eticlopride	D2	>1000
Vesamicol	VAChT	>1000

Table 2

Kinetics parameters of [^{11}C]**TZ1964B** PET brain imaging in NHPs at baseline

Regions	Kinetics parameters			
	LoganREF	SRTM		
	BP_{ND}	BP_{ND}	R1	k_2 (min^{-1})
Striatum	3.96 ± 0.17	4.64 ± 0.47	1.06 ± 0.16	0.11 ± 0.02
Cerebellum	Reference			

(n= 6 scans)

Table 3

Test-retest variability (TRV) and coefficient of variation (CV) of [^{11}C]**TZ1964B** PET brain imaging in NHPs at baseline

Methods	$BP_{striatum}$-test (mean ± SD)	CV (%)	$BP_{striatum}$-retest (mean ± SD)	CV (%)	Mean change (|%|)	TRV (% ± SD)
LoganREF	3.93 ± 0.0025	0.063	4.12 ± 0.063	1.52	4.80	4.62±1.59
SRTM	4.34 ± 0.23	2.27	4.94 ± 0.10	2.07	13.80	13.10±3.19

(n = 2 subjects, first 2 scans of each subject were included)

Table 4

Kinetic parameters of [^{11}C]**TZ1964B** PET brain imaging in NHPs following pharmacological pretreatment

Doses of MP-10 (mg/kg)	Kinetic parameters (Striatum)					
	LoganREF		SRTM			
	BP_{ND}	Occ%	BP_{ND}	R1	k_2 (min^{-1})	Occ %
2.00	0.4231	89.23	0.6558	1.0209	0.04245	86.65
1.50	0.4234	89.17	0.5732	0.8844	0.08179	80.00
1.00	0.8980	77.14	0.9026	0.9932	0.05868	81.63
0.50	0.8214	79.09	1.3084	0.7716	0.08542	73.37
0.25	2.8957	26.26	3.8161	1.0628	0.08540	22.32
0.10	3.7678	4.06	4.0338	1.1128	0.10847	17.79
0.05	3.7307	5.01	4.0253	0.9354	0.09479	18.07